Seismic interferometry, the optical theorem and a non-linear point diffractor

Kees Wapenaar, Department of Geotechnology, Delft University of Technology

SUMMARY

We analyze seismic interferometry for the response of a single point diffractor. By writing each of the Green's functions involved in the correlation process as a superposition of a direct wave and a scattered wave, the interferometric relations are rewritten as a superposition of four terms. Starting with a model based on the Born approximation, we show that a three term approximation yields a nearly exact result, whereas the full four term expression results in a significant non-physical event. For the correct, non-linear diffractor model, it appears that the result of the three term approximation contains a non-physical event, which disappears by taking all four terms into account.

INTRODUCTION

The aim of this paper is to discuss seismic interferometry for the response of a single point diffractor. We start by reviewing the Green's function representation for interferometry. Next we apply this to the response of a point diffractor and show that this leads to a paradox when the diffractor is modeled with the Born approximation. We show that the paradox is resolved if we use a non-linear model for the point diffractor.

In the space-frequency domain $(\mathbf{x},\omega)$, the general Green's function representation for seismic interferometry is given by

$$2\Re\{\hat{G}(\mathbf{x}_B,\mathbf{x}_A,\omega)\} = \oint_{\partial\mathbb{D}} \frac{-1}{j\omega\rho(\mathbf{x})}\Big(\hat{G}^*(\mathbf{x}_A,\mathbf{x},\omega)\partial_i\hat{G}(\mathbf{x}_B,\mathbf{x},\omega) - \big(\partial_i\hat{G}^*(\mathbf{x}_A,\mathbf{x},\omega)\big)\hat{G}(\mathbf{x}_B,\mathbf{x},\omega)\Big)n_i\,\mathrm{d}^2\mathbf{x}, \quad (1)$$

where $\partial\mathbb{D}$ is a closed surface with outward pointing normal vector $\mathbf{n}=(n_1,n_2,n_3)$, $\hat{G}(\mathbf{x}_B,\mathbf{x}_A,\omega)$ is the Green's function at angular frequency ω between points $\mathbf{x}_A$ and $\mathbf{x}_B$ inside $\partial\mathbb{D}$, $\rho(\mathbf{x})$ is the mass density, j is the imaginary unit, superscript * denotes complex conjugation and $\Re$ denotes the real part. This representation is exact for arbitrary inhomogeneous, lossless media (Wapenaar et al., 2005).

For later convenience we consider a slightly different form of the Green's function representation. To this end we introduce a modified Green's function $\hat{\mathcal{G}} = \frac{1}{j\omega}\hat{G}$. With this definition, equation 1 becomes

$$2j\Im\{\hat{\mathcal{G}}(\mathbf{x}_B,\mathbf{x}_A,\omega)\} = \oint_{\partial\mathbb{D}} \frac{1}{\rho(\mathbf{x})}\Big(\hat{\mathcal{G}}^*(\mathbf{x}_A,\mathbf{x},\omega)\partial_i\hat{\mathcal{G}}(\mathbf{x}_B,\mathbf{x},\omega) - \big(\partial_i\hat{\mathcal{G}}^*(\mathbf{x}_A,\mathbf{x},\omega)\big)\hat{\mathcal{G}}(\mathbf{x}_B,\mathbf{x},\omega)\Big)n_i\,\mathrm{d}^2\mathbf{x}, \quad (2)$$

where $\Im$ denotes the imaginary part (van Manen et al., 2005). Throughout this paper we assume that $\partial\mathbb{D}$ is a sphere with large radius and its center at the origin, and we assume that the medium outside this sphere is homogeneous. Using the equation of motion and far field assumptions, equation 2 thus becomes

$$2j\Im\{\hat{\mathcal{G}}(\mathbf{x}_B,\mathbf{x}_A,\omega)\} = \frac{-2j\omega}{\rho c}\oint_{\partial\mathbb{D}} \hat{\mathcal{G}}^*(\mathbf{x}_A,\mathbf{x},\omega)\hat{\mathcal{G}}(\mathbf{x}_B,\mathbf{x},\omega)\mathrm{d}^2\mathbf{x}, \quad (3)$$

where ρ and c are the constant mass density and propagation velocity of the medium outside the sphere. In the time domain, this last equation becomes

$$\mathcal{G}(\mathbf{x}_B,\mathbf{x}_A,t) - \mathcal{G}(\mathbf{x}_B,\mathbf{x}_A,-t) = \frac{-2}{\rho c}\frac{\partial}{\partial t}\oint_{\partial\mathbb{D}} \mathcal{G}(\mathbf{x}_A,\mathbf{x},-t) * \mathcal{G}(\mathbf{x}_B,\mathbf{x},t)\mathrm{d}^2\mathbf{x}, \quad (4)$$

where $*$ denotes convolution. The Green's functions on the right-hand side are the responses of a source at $\mathbf{x}$ at the closed surface $\partial\mathbb{D}$, observed by receivers at $\mathbf{x}_A$ and $\mathbf{x}_B$. The right-hand side involves cross-correlating these responses at $\mathbf{x}_A$ and $\mathbf{x}_B$, integrating over all sources at $\partial\mathbb{D}$, and taking the time-derivative of the result. According to equation 4, this gives the Green's function for a source at $\mathbf{x}_A$ and a receiver at $\mathbf{x}_B$, minus its time-reversed version. The right-hand side can be further simplified for a distribution of uncorrelated noise sources on $\partial\mathbb{D}$, but this is beyond the scope of this paper.

APPLICATION TO A POINT DIFFRACTOR

In the following we consider a point diffractor at the origin, embedded in an otherwise homogeneous medium with mass density ρ and propagation velocity c. We write for the Green's function

$$\hat{\mathcal{G}}(\mathbf{x}_B,\mathbf{x}_A,\omega) = \hat{\bar{\mathcal{G}}}(\mathbf{x}_B,\mathbf{x}_A,\omega) + \hat{\mathcal{G}}^s(\mathbf{x}_B,\mathbf{x}_A,\omega), \quad (5)$$

where $\hat{\bar{\mathcal{G}}}(\mathbf{x}_B,\mathbf{x}_A,\omega)$ and $\hat{\mathcal{G}}^s(\mathbf{x}_B,\mathbf{x}_A,\omega)$ are the direct and scattered wave fields, respectively. The direct wave field in the embedding is given by

$$\hat{\bar{\mathcal{G}}}(\mathbf{x}_B,\mathbf{x}_A,\omega) = \frac{\rho}{4\pi}\frac{\exp\{-jk|\mathbf{x}_B-\mathbf{x}_A|\}}{|\mathbf{x}_B-\mathbf{x}_A|}, \quad (6)$$

in 3D, with $k=\omega/c$, or

$$\hat{\bar{\mathcal{G}}}(\mathbf{x}_B,\mathbf{x}_A,\omega) = -\frac{j\rho}{4}H_0^{(2)}(k|\mathbf{x}_B-\mathbf{x}_A|), \quad (7)$$

in 2D, where $H_0^{(2)}$ is the zeroth order Hankel function of the second kind. The scattered wave field can be written as

$$\hat{\mathcal{G}}^s(\mathbf{x}_B,\mathbf{x}_A,\omega) = \hat{\bar{\mathcal{G}}}(\mathbf{x}_B,\mathbf{0},\omega)\hat{d}(\omega)\hat{\bar{\mathcal{G}}}(\mathbf{0},\mathbf{x}_A,\omega), \quad (8)$$

where $\hat{d}(\omega)$ is the diffraction coefficient of the point diffractor. Substitution of equation 5 and similar expressions for the other Green's functions into equation 3 gives

$$2j\Im\{\hat{\mathcal{G}}(\mathbf{x}_B,\mathbf{x}_A,\omega)\} = \hat{T}_1+\hat{T}_2+\hat{T}_3+\hat{T}_4, \quad (9)$$

where

$$\hat{T}_1 = \oint_{\partial\mathbb{D}} -\frac{2j\omega}{\rho c}\hat{\bar{\mathcal{G}}}^*(\mathbf{x}_A,\mathbf{x},\omega)\hat{\bar{\mathcal{G}}}(\mathbf{x}_B,\mathbf{x},\omega)\mathrm{d}^2\mathbf{x}, \quad (10)$$

$$\hat{T}_2 = \oint_{\partial\mathbb{D}} -\frac{2j\omega}{\rho c}\hat{\bar{\mathcal{G}}}^*(\mathbf{x}_A,\mathbf{x},\omega)\hat{\mathcal{G}}^s(\mathbf{x}_B,\mathbf{x},\omega)\mathrm{d}^2\mathbf{x}, \quad (11)$$

$$\hat{T}_3 = \oint_{\partial\mathbb{D}} -\frac{2j\omega}{\rho c}\hat{\mathcal{G}}^{s,*}(\mathbf{x}_A,\mathbf{x},\omega)\hat{\bar{\mathcal{G}}}(\mathbf{x}_B,\mathbf{x},\omega)\mathrm{d}^2\mathbf{x}, \quad (12)$$

$$\hat{T}_4 = \oint_{\partial\mathbb{D}} -\frac{2j\omega}{\rho c}\hat{\mathcal{G}}^{s,*}(\mathbf{x}_A,\mathbf{x},\omega)\hat{\mathcal{G}}^s(\mathbf{x}_B,\mathbf{x},\omega)\mathrm{d}^2\mathbf{x}. \quad (13)$$

BORN APPROXIMATION

We illustrate these expressions with a 2D numerical experiment. Figure 1 shows the configuration. 720 sources are equally distributed along a circle with a radius of 500 m and its center at the origin. The receiver coordinates are $\mathbf{x}_A = (0, -150)$ and $\mathbf{x}_B = (200, 0)$. The propagation velocity of the homogeneous embedding is $c = 1500$ m/s. The point diffractor at the origin is denoted by the star. It is modeled as a contrast in compressibility, according to $\Delta\kappa(\mathbf{x}) = \Delta\kappa_0\delta(\mathbf{x})$. In the Born approximation, the diffraction coefficient is thus given by $\hat{d}(\omega) = \omega^2\Delta\kappa_0$.

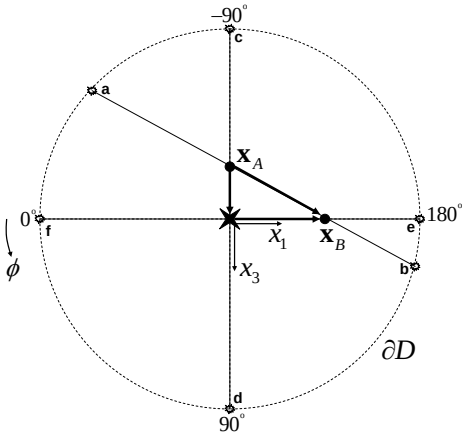

Fig. 1: *Single point diffractor in a homogeneous embedding. The receivers are at $\mathbf{x}_A$ and $\mathbf{x}_B$. The numerical integration is carried out along the sources at surface $\partial\mathbb{D}$. The main contributions come from the stationary points a, b, c, and e.*

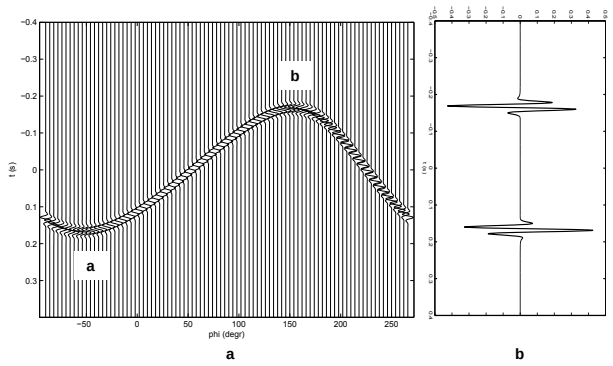

Fig. 2: *(a) Time domain representation of the integrand of equation 10. (b) The sum of all traces in (a). These events represent the direct wave $\bar{\mathcal{G}}(\mathbf{x}_B, \mathbf{x}_A, t)$ and its time-reversed version $-\bar{\mathcal{G}}(\mathbf{x}_B, \mathbf{x}_A, -t)$.*

The evaluation of equation 10 is illustrated in Figure 2. Figure 2a shows the integrand in the time domain. Each trace is the result of a cross-correlation of the direct waves $\bar{\mathcal{G}}(\mathbf{x}_A, \mathbf{x}, t)$ and $\bar{\mathcal{G}}(\mathbf{x}_B, \mathbf{x}, t)$ for one specific source position $\mathbf{x}$ at the surface $\partial\mathbb{D}$. The source coordinate is represented by the angle ϕ (conform its definition in Figure 1). Note that the Green's functions have been convolved with a Ricker wavelet with a central frequency of 50 Hz and that the correlation result has been differentiated with respect to time. Figure 2b shows the

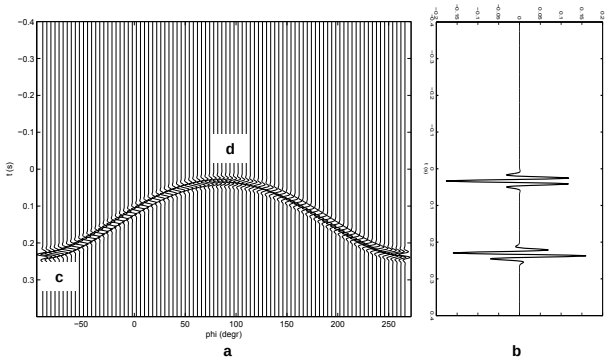

Fig. 3: *(a) Time domain representation of the integrand of equation 11. (b) The sum of all traces in (a). The event at 0.233 s represents the scattered Green's function $\mathcal{G}^s(\mathbf{x}_B, \mathbf{x}_A, t)$; the event at 0.033 s has no physical meaning.*

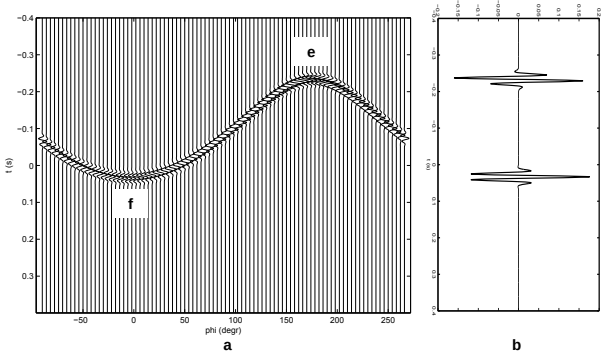

Fig. 4: *(a) Time domain representation of the integrand of equation 12. (b) The sum of all traces in (a). The event at -0.233 s represents the time-reversed scattered Green's function $-\mathcal{G}^s(\mathbf{x}_B, \mathbf{x}_A, -t)$; the event at 0.033 s has no physical meaning.*

result of the integration. The main contributions come from the Fresnel zones around the stationary points denoted by 'a' and 'b' in Figures 1 and 2a. The two events in Figure 2b correspond to the direct wave $\bar{\mathcal{G}}(\mathbf{x}_B, \mathbf{x}_A, t)$ and its time-reversed version $-\bar{\mathcal{G}}(\mathbf{x}_B, \mathbf{x}_A, -t)$. The arrival times are $\pm t_{AB}$, with $t_{AB} = |\mathbf{x}_B - \mathbf{x}_A|/c = 0.167$ s.

Figure 3a is the time domain representation of the integrand of equation 11. The first stationary point, denoted by 'c', occurs at $\phi = -90^o$. For this source both Green's functions $\bar{\mathcal{G}}(\mathbf{x}_A, \mathbf{x}, t)$ and $\mathcal{G}^s(\mathbf{x}_B, \mathbf{x}, t)$ have the path from $\mathbf{x}$ to $\mathbf{x}_A$ in common, hence, in the cross-correlation process the travel time from $\mathbf{x}$ to $\mathbf{x}_A$ is subtracted from that of the scattered Green's function $\mathcal{G}^s(\mathbf{x}_B, \mathbf{x}, t)$. The remaining travel time is $t_A + t_B = (|\mathbf{x}_A| + |\mathbf{x}_B|)/c = 0.233$ s, which is the travel time of the arrival in the scattered Green's function $\mathcal{G}^s(\mathbf{x}_B, \mathbf{x}_A, t)$. Hence, the arrival at 0.233 s in Figure 3b represents $\mathcal{G}^s(\mathbf{x}_B, \mathbf{x}_A, t)$. The second stationary point in Figure 3a, denoted by 'd', occurs at $\phi = +90^o$. For this source, the travel time of the correlation result is $t_B - t_A = (|\mathbf{x}_B| - |\mathbf{x}_A|)/c = 0.033$ s. The arrival at 0.033 s in Figure 3b has no physical meaning.

Figure 4a is the time domain representation of the integrand of equation 12. At the stationary point, denoted by 'e', the Green's functions $\mathcal{G}^s(\mathbf{x}_A, \mathbf{x}, t)$ and $\bar{\mathcal{G}}(\mathbf{x}_B, \mathbf{x}, t)$ have the path from $\mathbf{x}$ to $\mathbf{x}_B$ in common. The travel time of the correlation

result is $-(t_A + t_B) = -0.233$ s. The arrival at this travel time in Figure 4b represents the time-reversed scattered Green's function $-\mathcal{G}^s(\mathbf{x}_B, \mathbf{x}_A, -t)$. The stationary point denoted by 'f' contributes to the non-physical arrival at 0.033 s in Figure 4b. Note that this arrival is opposite in sign compared to the arrival at 0.033 s in Figure 3b.

We now superpose the results of equations 10, 11 and 12. Figure 5 shows the sum of the results in Figures 2, 3 and 4. The events in Figure 5b are $\bar{\mathcal{G}}(\mathbf{x}_B, \mathbf{x}_A, t) - \bar{\mathcal{G}}(\mathbf{x}_B, \mathbf{x}_A, -t) + \mathcal{G}^s(\mathbf{x}_B, \mathbf{x}_A, t) - \mathcal{G}^s(\mathbf{x}_B, \mathbf{x}_A, -t)$. Note that the non-physical arrivals at 0.033 s canceled each other. Hence, the result in Figure 5b represents the complete Green's function between $\mathbf{x}_A$ and $\mathbf{x}_B$, minus its time-reversed version, i.e., $\mathcal{G}(\mathbf{x}_B, \mathbf{x}_A, t) - \mathcal{G}(\mathbf{x}_B, \mathbf{x}_A, -t)$. Figure 6 shows again the result of Figure 5b, together with the directly modeled Green's function between $\mathbf{x}_A$ and $\mathbf{x}_B$. The match is nearly perfect.

Finally we evaluate equation 13. The scattered Green's functions $\mathcal{G}^s(\mathbf{x}_A, \mathbf{x}, t)$ and $\mathcal{G}^s(\mathbf{x}_B, \mathbf{x}, t)$ have the path from $\mathbf{x}$ to the point diffractor in common *for all* $\mathbf{x}$. Hence, the travel time of the correlation result is equal to $t_B - t_A = (|\mathbf{x}_B| - |\mathbf{x}_A|)/c = 0.033$ s for all $\mathbf{x}$, see Figure 7a. The integration result is shown in Figure 7b. Note that the amplitude of this non-physical event is stronger than any of the physical events in Figure 6. Following equation 9, we add this result to the other three terms and compare it again with the modeled Green's function, see Figure 8.

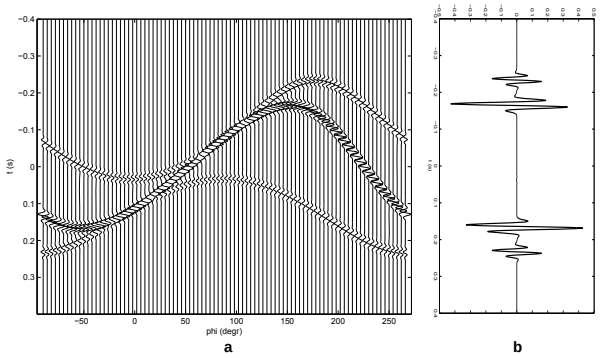

Fig. 5: *(a) Superposition of Figures 2a, 3a and 4a. (b) The sum of all traces in (a). This represents the complete Green's function between* $\mathbf{x}_A$ *and* $\mathbf{x}_B$*, minus its time-reversed version, i.e.,* $\mathcal{G}(\mathbf{x}_B, \mathbf{x}_A, t) - \mathcal{G}(\mathbf{x}_B, \mathbf{x}_A, -t)$.

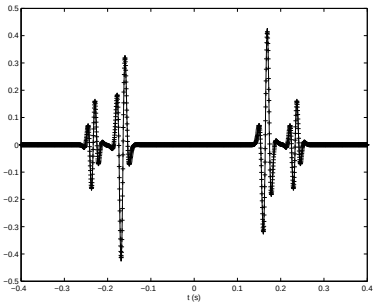

Fig. 6: *Three-term approximation of equation 9 (i.e., the result of Figure 5b, here denoted by the solid line), compared with the directly modeled Green's function between* $\mathbf{x}_A$ *and* $\mathbf{x}_B$ *(denoted by the +signs).*

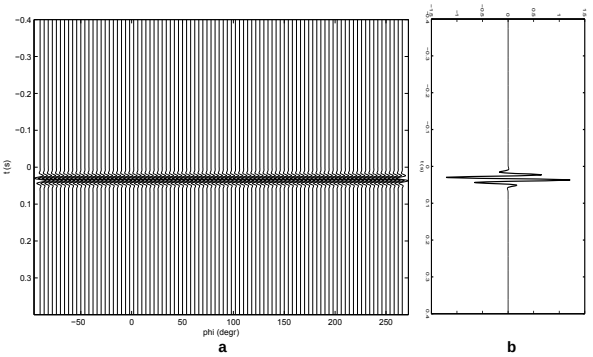

Fig. 7: *(a) Time domain representation of the integrand of equation 13. (b) The sum of all traces in (a). The event at 0.233 s has no physical meaning.*

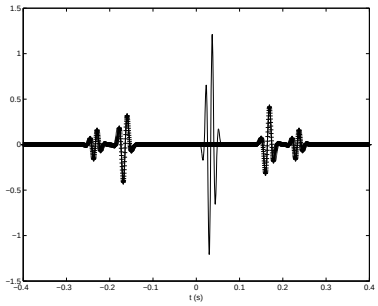

Fig. 8: *All four terms of equation 9 (i.e., the result of Figure 6, with the non-physical event of Figure 7b added to it), compared with the directly modeled Green's function between* $\mathbf{x}_A$ *and* $\mathbf{x}_B$ *(denoted by the +signs).*

A PARADOX

From the analysis in the previous section it appears that taking only three of the four terms of equations $10 - 13$ into account leads to a better retrieval of the Green's function (Figure 6) then when all terms are taken into account, as prescribed by the theory (Figure 8). In most practical situations it will not be possible to do the cross-correlation term-by-term: when the full responses are cross-correlated the fourth term is automatically included. Apart from this practical issue, a more intriguing question is how it is possible that the three-term approximation leads to a better result than the full four term expression.

The answer is that we used the Born approximation to model the point diffractor. This approximation implies that we only consider first order scattering at the diffractor, so in order to be consistent we should only consider terms up to first order scattering. Equations $10 - 12$ obey this condition, but equation 13 describes the cross-correlation of two scattered Green's functions, so this term is proportional to second order scattering and should be omitted in this analysis. Apparently we should go beyond Born modeling of the point diffractor if we want to get a consistent result when all four terms of equation 9 are taken into account.

Snieder et al. (2008) analyzed integrals like those in equations $10 - 13$ by the method of stationary phase for the situation of an arbitrary scattering object with compact support around the origin. They showed that the non-physical events in the three integrals $11 - 13$ cancel each other on account of the

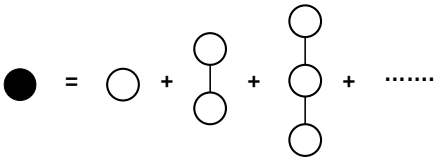

Fig. 9: *Diagrammatic representation of the non-linear diffraction coefficient (after Snieder, 1999). The single line denotes the regularized Green's function $j\Im\{\hat{\tilde{\mathcal{G}}}(\mathbf{0},\mathbf{0},\omega)\}$. The open circle denotes the coefficient $\hat{u}$ and the black circle stands for the non-linear diffraction coefficient $\hat{d}$.*

generalized optical theorem (Glauber and Schomaker, 1953) and thus solved the paradox.[1] Halliday and Curtis (2009) applied a similar analysis for surface waves. In the following we show the implications for the point diffractor response.

A NON-LINEAR DIFFRACTOR MODEL

We will use the optical theorem to derive a better model for a point diffractor. For an omnidirectional scatterer the generalized optical theorem (Glauber and Schomaker, 1953) simplifies to

$$-\Im(f) = k|f|^2, \tag{14}$$

where f is the scattering coefficient (the minus-sign on the left-hand side is usually absent; it stems from our definition of the temporal Fourier transform). Because of the factor $\rho/4\pi$ in equation 6 in our definition of the 3D Green's function, our diffraction coefficient $\hat{d}(\omega)$ in equation 8 is related to f via $\hat{d}(\omega) = \frac{4\pi}{\rho} f$, which leads to the following modified version of the optical theorem for a point diffractor in 3D space

$$-\Im(\hat{d}) = \frac{k\rho}{4\pi}\,|\hat{d}|^2. \tag{15}$$

Similarly, for a point diffractor in 2D space we have

$$-\Im(\hat{d}) = \mathrm{sgn}(\omega)\,\frac{\rho}{4}\,|\hat{d}|^2. \tag{16}$$

These equations are solved by

$$\hat{d} = \frac{\hat{u}}{1 + j\hat{u}\frac{k\rho}{4\pi}} \quad \text{(3D)}, \tag{17}$$

and

$$\hat{d} = \frac{\hat{u}}{1 + j\hat{u}\,\mathrm{sgn}(\omega)\rho/4} \quad \text{(2D)}, \tag{18}$$

respectively, where $\hat{u}$ is still an undetermined quantity. Using $\Im\{\hat{\tilde{\mathcal{G}}}(\mathbf{0},\mathbf{0},\omega)\} = -\frac{k\rho}{4\pi}$ (3D; equation 6), or $\Im\{\hat{\tilde{\mathcal{G}}}(\mathbf{0},\mathbf{0},\omega)\} = -\mathrm{sgn}(\omega)\rho/4$ (2D; equation 7), we may rewrite both equations 17 and 18 as

$$\hat{d} = \frac{\hat{u}}{1 - \hat{u}\hat{\tilde{\mathcal{G}}}_0^{\mathrm{reg}}} = \hat{u} + \hat{u}\hat{\tilde{\mathcal{G}}}_0^{\mathrm{reg}}\hat{u} + \hat{u}\hat{\tilde{\mathcal{G}}}_0^{\mathrm{reg}}\hat{u}\hat{\tilde{\mathcal{G}}}_0^{\mathrm{reg}}\hat{u} + \cdots, \tag{19}$$

where $\hat{\tilde{\mathcal{G}}}_0^{\mathrm{reg}}$ stands for $j\Im\{\hat{\tilde{\mathcal{G}}}(\mathbf{0},\mathbf{0},\omega)\}$. Note that, whereas $\hat{\tilde{\mathcal{G}}}(\mathbf{0},\mathbf{0},\omega)$ diverges, its imaginary part is finite, which is why

[1] We can also turn the argument: since the interferometric representation 3 is correct, the non-physical events must vanish, hence the optical theorem follows from equation 3.

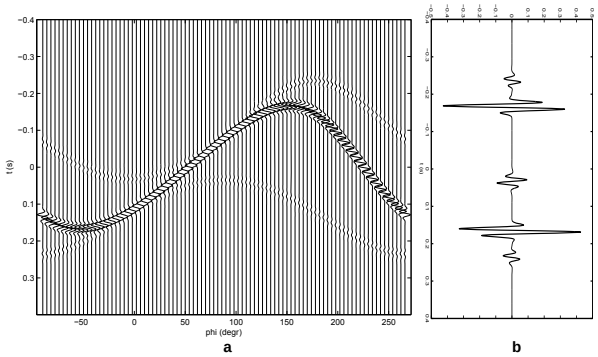

Fig. 10: *(a) Three-term approximation, as in Figure 5a, but this time for the non-linear diffractor model of equation 19. (b) The sum of all traces in (a). Note that the non-physical events at $t_B - t_A = 0.033$ s do not cancel.*

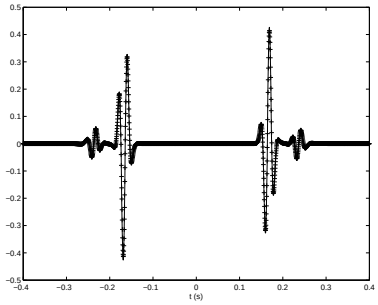

Fig. 11: *All four terms of equation 9, as in Figure 8, but this time for the non-linear diffractor model of equation 19. Note that the fourth term canceled the non-physical event of Figure 10b.*

$\hat{\tilde{\mathcal{G}}}_0^{\mathrm{reg}}$ is called the regularized Green's function (van Rossum and Nieuwenhuizen, 1999). The series expansion in equation 19 clearly shows that the coefficient $\hat{d}$ accounts for primary and multiple scattering at the point diffractor, see Figure 9. It can be seen as the 3D (or 2D) complement of a 1D expression discussed by (Snieder, 1999). The first term of this expansion represents the Born approximation, hence for a contrast in compressibility we take $\hat{u} = \omega^2\Delta\kappa_0$.

We repeat the numerical experiments, this time using the non-linear diffractor model of equation 19. Figure 10 shows the result of the three term approximation, analogous to Figure 5. Note that the non-physical events at $t_B - t_A = 0.033$ s resulting from equations 11 and 12 do not cancel. Unlike in Figures 3 and 4, where these events showed a zero-phase behavior, here they are not zero-phase as a result of the complex-valued diffraction coefficient and therefore they do not cancel. By adding the fourth term, resulting from the cross-correlation of the scattered Green's functions (equation 13), the non-physical event is canceled, as shown in Figure 11.

CONCLUSIONS

We have shown that the Born approximation is an insufficient model to explain all aspects of seismic interferometry applied to the response of a single point diffractor. Via the generalized optical theorem we arrived at a more advanced, non-linear diffractor model and showed that with this model seismic interferometry retrieves the scattered Green's function very well.

References

Glauber, R. and V. Schomaker, 1953, The theory of electron diffraction: Phys. Rev., **89**, 667–671.

Halliday, D. and A. Curtis, 2009, A generalized optical theorem for surface waves and layered media: Phys. Rev. E., (submitted).

Snieder, R., 1999, Imaging and averaging in complex media., *in* Fouque, J. P., ed., Diffuse waves in complex media, 405–454, Kluwer.

Snieder, R., K. van Wijk, M. Haney, and R. Calvert, 2008, Cancellation of spurious arrivals in Green's function extraction and the generalized optical theorem: Phys. Rev. E., **78**, 036606.

van Manen, D.-J., J. O. A. Robertsson, and A. Curtis, 2005, Modeling of wave propagation in inhomogeneous media: Phys. Rev. Lett., **94**, 164301–1–164301–4.

van Rossum, M. C. W. and T. M. Nieuwenhuizen, 1999, Multiple scattering of classical waves: microscopy, mesoscopy, and diffusion: Rev. Mod. Phys., **71**, 313–371.

Wapenaar, K., J. Fokkema, and R. Snieder, 2005, Retrieving the Green's function in an open system by cross-correlation: a comparison of approaches (L): J. Acoust. Soc. Am., **118**, 2783–2786.